Localized intermittent short-wavelength bursts in the high-radius ratio limit of the Taylor-Couette system

C. S. Carey,[1] A. B. Schlender,[2] and C. D. Andereck[2]
[1]*Department of Physics, University of Wisconsin, Madison, Wisconsin, USA*
[2]*Department of Physics, The Ohio State University, Columbus, Ohio, USA*
(Received 5 May 2006; revised manuscript received 29 September 2006; published 16 January 2007)

We have explored flow states of the Taylor-Couette system in the high radius ratio limit (0.99) with only the inner cylinder rotating. The usual Taylor vortices and wavy vortices were found, but the transition to higher states is interrupted by the emergence of intermittent short-wavelength bursts. This flow state is distinct from previously observed bursting phenomena found at lower radius ratios, while it is similar in appearance to states found in inclined layer convection.

DOI: 10.1103/PhysRevE.75.016303 PACS number(s): 47.20.−k

I. INTRODUCTION

The Taylor-Couette system, which consists of the flow of a fluid in the gap between rotating concentric cylinders, is a paradigm in the study of pattern formation. The system exhibits a large variety of ordered and disordered behaviors, depending on fixed parameters such as the relative radii of the inner and outer cylinders, and on the two control parameters, the rotation speeds of the cylinders [1,2]. Considerable attention has been paid to realizations of the system in which the ratio of the radii of the two cylinders is less than 0.9. Recently, however, interest has grown in the behavior of the system for radius ratios approaching 1. The rationale for such studies is straightforward: As the radius ratio approaches 1, the geometry looks, locally, increasingly planar, and thus the behavior should approach that of plane Couette flow. Theoretical studies predict a transition region between circular and planar Couette flow [3,4]. Experiments have been performed that show the same phenomenon (periodic turbulent bands) in both circular and plane Couette flow for a radius ratio of 0.98 [5,6]. The present experiment was designed with the intent of moving farther into the transition region. For our initial effort in this direction we constructed a system with very large cylinders and with a radius ratio of 0.99. As will be shown, this leads to other behaviors.

To place our work in its proper context, it is helpful to review previous work in which bursting has been observed. For example, it has long been known that isolated bursts of *turbulent* flow can form and decay throughout the Taylor-Couette system against a background of *laminar* spirals for certain ranges of rotation speeds and cylinder radius ratios when the cylinders rotate in opposite directions [1,7]. For other radius ratios, bursting in which the entire flow periodically alternates between ordered laminar and turbulent behavior has been observed and modeled [8,9]. Bursting behavior of various other kinds has also been observed in binary-fluid convection [10,11], in wall-bounded shear flows [12], and in other nonlinear dynamical systems. One notable recent experiment has found a *nonturbulent* bursting behavior. Specifically, localized intermittent short-wavelength bursts of waves with a well-defined wave number were observed to occur on a background of persistent convection rolls in an inclined layer convection experiment [13]. Although inclined layer convection is a relatively simple pattern-forming system, a theoretical understanding of this particular bursting phenomenon has yet to emerge. We will describe a similar phenomenon found experimentally in the radius ratio 0.99 Taylor-Couette system.

II. EXPERIMENTAL APPARATUS AND PROCEDURES

The Taylor-Couette apparatus was constructed with concentric independently rotating cylinders. The radius of the outer cylinder is $r_o=29.84\pm0.01$ cm and that of the inner cylinder is $r_i=29.53\pm0.01$ cm. This gives a gap width between the cylinders of $d=r_o-r_i=0.31\pm0.02$ cm and a radius ratio of $\eta=r_i/r_o=0.990\pm0.001$. The outer cylinder was machined from clear acrylic plastic and the inner cylinder from a dark gray nylon.

To provide a precise lower boundary at the base of the fluid column, a ring was constructed of acrylic plastic and attached to the bottom of the outer cylinder. This ring nearly fills the gap between the cylinders. The upper boundary was left free. While the boundary conditions are asymmetric, the phenomena discussed here occur in the bulk of the fluid and should not be significantly affected by the details of the boundary conditions. The cylinder height accessible to the fluid is $h=13.9$ cm, giving an aspect ratio of $\Gamma=h/d=44.8$. An aspect ratio of this size indicates that the boundary conditions will not play a strong role in the bulk of the fluid. In addition, all data in this paper come from observations more than 2.5 cm from each boundary.

Compumotor stepper motors drive the rotation of the cylinders through worm gear speed reducers. The two independent control parameters are the inner cylinder Reynolds number $R_i=\frac{\Omega_i r_i d}{\nu}$, and the outer cylinder Reynolds number $R_o=\frac{\Omega_o r_o d}{\nu}$, where (Ω_i,Ω_o) is the (*inner, outer*) cylinder frequency and ν is the kinematic viscosity. In the present work only the inner cylinder rotates.

Visualization of the fluid motion is achieved by the addition of Kalliroscope AQ-1000 flakes to the working fluid [14,15]. For adequate visualization a concentration of approximately 3% by volume was used. The viscosity of the working fluid is $\nu=0.0098$ cm^2/sec at a temperature of 72 °F. The Kalliroscope fluid contains reflective polymer

platelets. The shear in the flow aligns the platelets [15]. Roughly speaking, axial or azimuthal flow exposes the reflective side of the platelets, creating a lighter region in the fluid, while radial flow exposes the edges of the platelets to view, revealing the nearly black inner cylinder, thus creating a darker region. By detecting the intensity of the light reflected by the platelets, one can infer the qualitative, and to some extent, quantitative, behavior of the fluid.

All data were acquired with a CCD array camera interfaced to a personal computer via a National Instruments 1424 image acquisition board. The camera is controlled by National Instruments LabView software. The images acquired by the CCD camera are used to create a space-time display of the fluid motion. This is achieved by extracting a vertical slice along the length of the cylinders, one pixel wide, from each frame acquired by the camera. Each line of pixels is appended to those preceding it to show the space-time evolution of the flow. The CCD camera runs at 28 frames per second and the shutter speed is $\frac{1}{1000}$ sec. The camera is fast enough to capture the phenomena discussed in the following sections in the space-time images without significant distortion. An example space-time image is shown in Fig. 1.

All data discussed here have been obtained by varying R_i while maintaining $R_o=0$. This line on the (R_o,R_i) plane has been systematically investigated by increasing the rotation rate of the inner cylinder quasistatically. A wait of at least four minutes after a change in R_i allows the system to reach a steady state before acquiring data. [Note that the axial viscous diffusion time is $\frac{h}{6\nu}\sim\frac{170}{6\times0.01}\sim50$ min. However, the transitions observed do not depend on ramping rate so far as we have been able to determine.]

III. EXPERIMENTAL RESULTS AND ANALYSIS

The flow states in low to moderate η Taylor-Couette systems have been mapped out in detail [16,2,1]. The primary flow state of this system, Couette flow, and the primary and secondary instabilities, Taylor vortex flow (TVF) and wavy vortex flow (WVF), respectively, are all observed in the large η Taylor-Couette system, although, of course, with different critical Reynolds numbers than for smaller η systems.

A. Taylor vortex flow

The onset of Taylor vortex flow is found to occur gradually over a broad range of Reynolds numbers. As with lower η systems, the initial appearance of TVF is found near the solid bottom boundary, in the form of a cell generated by Ekman pumping. The onset of vortices away from either bottom or top boundary, confined to a relatively narrow band, is found at $R_i=358$. Upon further increase of R_i, additional vortices gradually appear until they fill the entire system at $R_i=442$. Figure 2(a) shows a close-up view of this state. The axial wavelength of the vortices is 0.6 cm$=1.94d$, consistent with the behavior observed at lower η. Experimentally we find it difficult to obtain a completely defect-free state, and typically a slow, very long azimuthal wavelength oscillation of the vortices is present (visible in Fig. 1).

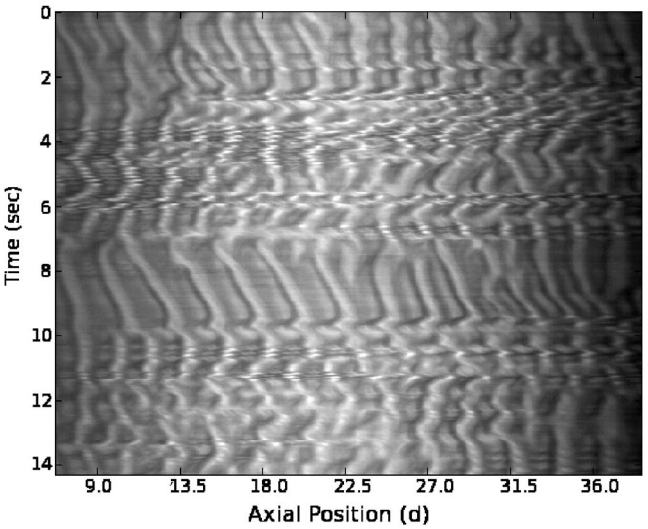

FIG. 1. Sample space-time image for $R_i=535$. The horizontal axis is given in units of the gap between the cylinders, d.

We attribute these difficulties to unavoidable slight imperfections in the apparatus relative to the very small gap.

B. Wavy vortex flow

The onset of wavy vortex flow occurs at $R_i=475$. In contrast with the TVF onset, this is a much more precisely defined transition. The waves are quite long in the azimuthal direction: the wavelength is approximately 7.5 cm, which implies that there are $m\sim25$ waves around the cylinders. Figure 2(b) shows a photograph of a typical state. For lower η systems it is normal to observe a multiplicity of m-states, depending upon the history of the flows. In the present case we have not attempted to determine what states the system can access, as we were primarily concerned with behavior at higher Reynolds numbers.

C. Very short wavelength bursting

Chaotic behavior for the $\eta=0.88$ system follows a transition from WVF to modulated wavy vortex flow (MWVF). In our $\eta=0.99$ system, the transition to MWVF is not observed. In its place we find an instability that we will call very short wavelength bursting (VSWB), with onset at $R_i=483$. The VSWB is characterized by high frequency small-wavelength (compared with the WVF waves that precede this state) ordered wavy patterns that appear in localized regions intermittently in space and time on the already formed persistent background of normal wavy vortices. The azimuthal wavelength of the VSWB is approximately 1.9 cm. As R_i is increased from 483 the frequency of formation and lifetime of the VSWB increases until the bursts nearly saturate the system at $R_i=900$.

To analyze the space-time data from this flow state it is necessary to distinguish between the bursts of interest and the surrounding background flow. Visually this is not difficult, as illustrated by comparing Fig. 1 with Fig. 3. We have automated the process by producing a binary version of the

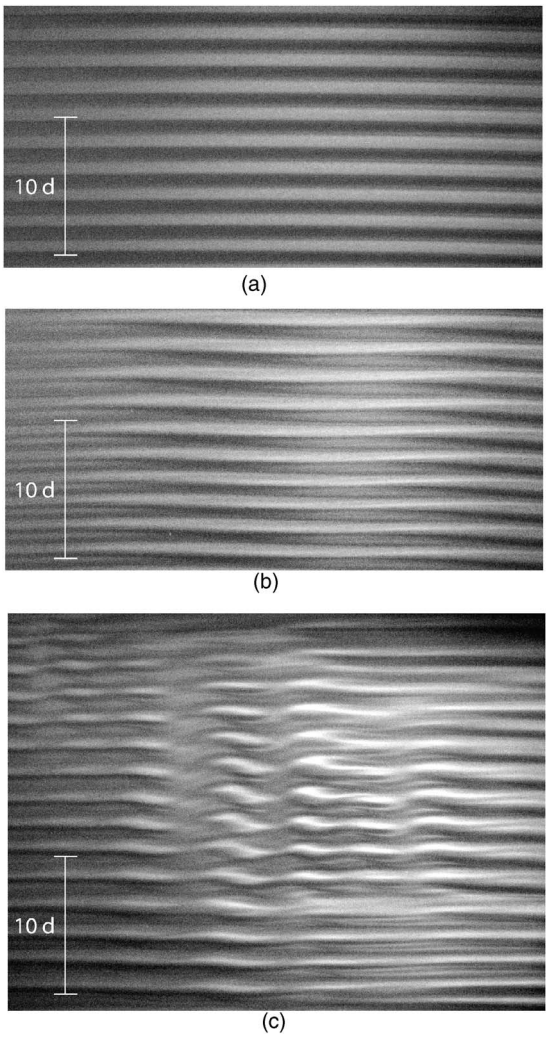

FIG. 2. Images of the primary instabilities of the high radius ratio Taylor-Couette system. The vertical direction is along the system's axis, while the horizontal dimension is along the circumference of the system. A scale is provided for reference, in units of the gap between the cylinders d. (a) Taylor vortex flow at R_i=450. (b) Wavy vortex flow at R_i=480. (c) Very short wavelength burst at R_i=530.

space-time data [17]. Because the bursts in which we are interested have a distinct frequency component we have chosen to use a frequency-based discrimination scheme [7]. The procedure involves stepping a 16 point window in the temporal direction. On each step the power spectrum of the temporal line at each spatial point is calculated. The power of three predetermined Fourier frequencies is compared to a cutoff value. If the power of one of these frequencies is above the cutoff value the first point in the temporal line is labeled as inside a burst. The cutoff value of the frequency power is tuned by hand to ensure that the bursts are captured.

The filtering algorithm is not perfect, of course, and therefore a massaging routine has been applied to the data to remove spurious burst and background points [17]. On a first pass through the data, burst points without two nearest neighbor points that are also in a burst are relabeled as background. In the second pass the background points that have

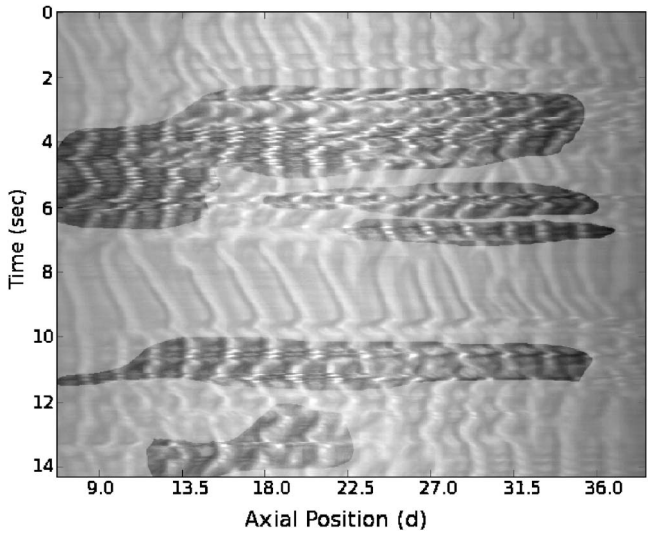

FIG. 3. Version of space-time image shown in Fig. 1 in which the high frequency regions of the flow indicating the presence of VSWB have been highlighted. The horizontal axis is given in units of the gap between the cylinders, d.

three nearest neighbors that are in a burst are relabeled as belonging to that burst. The third pass is similar to the first, but burst points must now have a minimum of three nearest neighbors that are burst points to remain a burst point. For the fifth pass, if spatial point i is in a burst and spatial point i+5 is in a burst, all of the points in between them are relabeled as burst points. The next pass over the data is similar, but checks the fifth point in time, and the last pass is the same as the fifth pass. The results of filtering a space-time image using this method can be seen in Fig. 4. Here the VSWB pixels are displayed in white and the background pixels are displayed in black.

To quantify the development of VSWB with increasing R_i the fraction of the system in bursts, f_B, has been calculated.

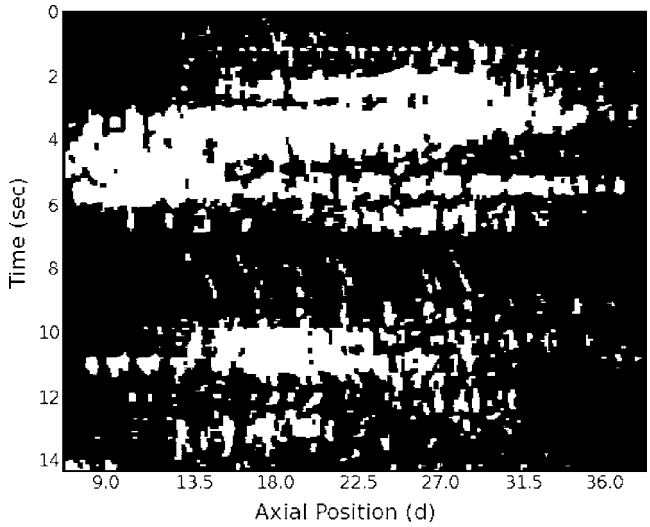

FIG. 4. Binarized version of space-time image shown in Fig. 1. White pixels indicate the presence of the VSWB. Black pixels indicate background flow. The horizontal axis is given in units of the gap between the cylinders, d.

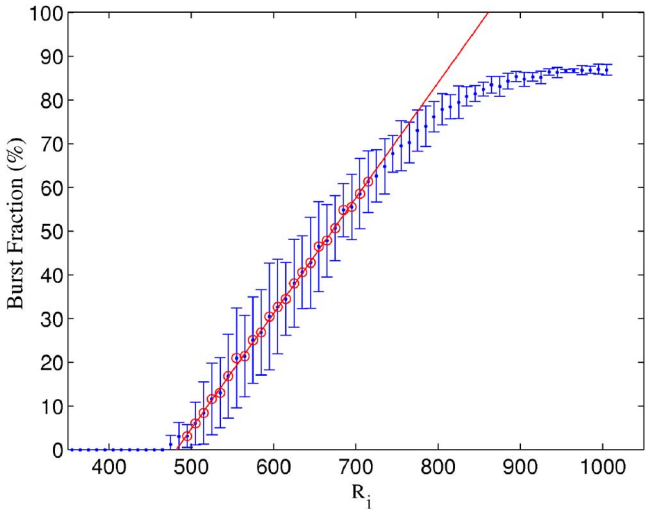

FIG. 5. (Color online) Burst fraction as a function of R_i. A linear fit indicates that the onset of the VSWB occurs at $R_i \approx 482$.

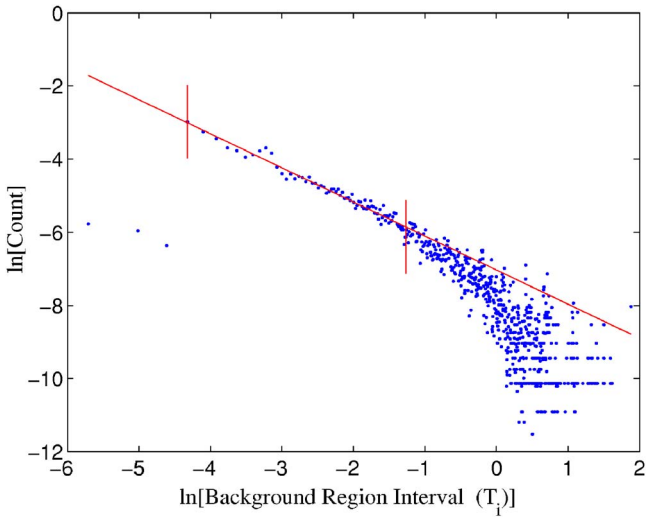

FIG. 6. (Color online) Distribution of the background region sizes in the algebraic regime at $R_i=545$. Background region length is given in units of the inner cylinder period, T_i. A fit to the data between the vertical lines gives an algebraic dependence with a characteristic exponent of $\mu \sim 0.93$.

f_B is defined to be the percentage of pixels in the binarized space-time image that are determined to be in the bursts. A plot of f_B as a function of R_i can be seen in Fig. 5. A linear fit to f_B confirms that the transition to the VSWB begins at $R_i \approx 482$. A small increase in f_B prior to $R_i=482$ is observed. This effect may be due to unavoidable imperfections in the gap width of the system. The VSWB saturates at $R_i \approx 900$.

In an attempt to further characterize the VSWB, the evolution of the temporal length of the background regions (i.e., outside the bursts), in the filtered space-time images has been investigated [18]. (Note that the following procedure parallels that applied to bursting and spatial-temporal intermittency in which the burst itself is turbulent and the background is laminar—in our case, both the burst and the background are laminar, but very distinct in character.) The analysis proceeds by constructing a histogram of the background lengths in time, $N(l)$, for each binary space-time image. A gradual transition is observed in the behavior of $N(l)$ as R_i is increased. For values of R_i just above the critical value for the onset of the VSWB, $N(l)$ is observed to have an algebraic dependence as $N(l) \propto l^{-\mu}$, where the characteristic exponent is $\mu \sim 0.93$. This is a result of the bursting nature of the VSWB. The algebraic dependence of $N(l)$ indicates that the background regions appear in the system on all length scales because the VSWB appears spontaneously and randomly leaving random lengths of background behavior. For larger values of the inner Reynolds number, above $R_i \approx 575$, $N(l)$ gradually becomes exponential, $N(l) \propto e^{-l/\tau}$. The characteristic time is $\tau \sim 0.038 T_i$, where T_i is the period of the inner cylinder. The exponential dependence indicates that the VSWB are beginning to dominate the system and the lengths of the background regions are becoming small rapidly. τ varies as a power law with R_i, with exponent $\alpha \approx 0.30$. Examples of $N(l)$ in the algebraic and exponential regimes can be seen in Figs. 6 and 7. These results are consistent with spatial-temporal intermittent behavior observed in, for example, the Taylor-Dean system [17], the counter-rotating Taylor-Couette system at lower η [7], convection in an annulus [19], directional viscous fingering [20], and, of course, in model systems [18]. The particular values for the scaling behavior and exponents vary among the systems (see [17], which tabulates the values for various systems, with μ ranging from 0.61 to 2.0 and α ranging from 0.5 to 0.73), but the general behavioral character (i.e., a transition from algebraic to exponential distributions as the control parameter is increased) is consistent from system to system.

IV. DISCUSSION AND CONCLUSIONS

Faisst and Eckhardt [4] discuss the precise conditions under which one may reasonably expect to find a transition

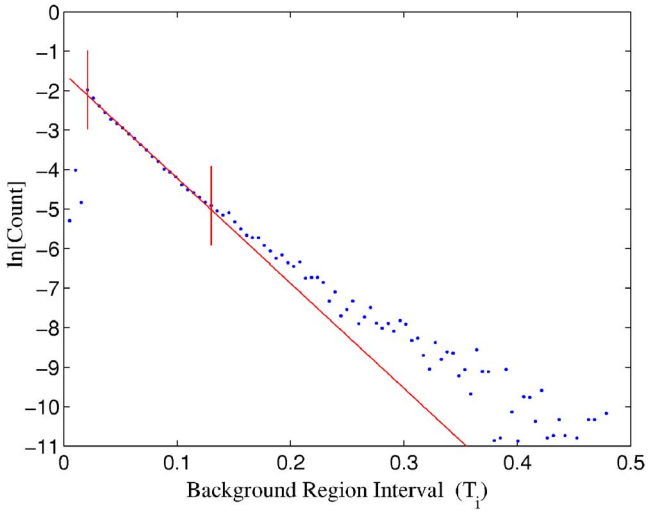

FIG. 7. (Color online) Distribution of the background region sizes in the exponential regime at $R_i=855$. Background region length is given in units of the inner cylinder period, T_i. A fit to the data between the vertical lines gives an exponential dependence with a characteristic length of $\tau \sim 0.038 T_i$.

between Taylor-Couette and plane Couette flow instabilities. They study numerically the radius ratio range above 0.90 and find significant deviations in the primary instabilities from the Taylor-Couette case. In particular, they predict that for $\eta=0.99$ and the outer cylinder at rest one should expect to see a crossover between Taylor vortices and wavy Taylor vortices as the primary instability. At higher values of η (~ 0.999) they find that there should be a point at which the linear instabilities characterizing Taylor-Couette flow give way to the subcritical behaviors found in plane Couette flow, again for the outer cylinder at rest. It is very unlikely that experiments will be able to reach this limit with only the inner cylinder rotating, but with the outer cylinder rotating the requirements are much less stringent and the transition to plane Couette phenomena in a cylindrical system may be realizable. The apparatus discussed here has the potential to achieve this.

Despite not achieving the conditions called for by Faisst and Eckhardt [4], the experiments reported here have nonetheless shown that for a Taylor-Couette apparatus with $\eta \sim 0.99$ and the outer cylinder stationary, the behavior of the system already differs significantly from that observed at lower values of η. These differences are observed above onset, in a regime not described theoretically at this time: Taylor vortices form as the initial instability, followed by wavy vortices. However, the flow changes to a background of wavy vortices with intermittent short-wavelength bursts shortly above the onset of the wavy vortex flow. The flow cannot sustain patterns with axial and azimuthal periodicity for high Reynolds numbers, thus truncating the sequence of ordered states found, for example, in the more commonly studied $\eta=0.88$ system. Although we find bursting as we approach the plane Couette flow limit, the bursting is superficially reminiscent of that seen in plane Couette flow, the onset is supercritical rather than subcritical as expected for plane Couette flow. The bursting we observe shares scaling characteristics with other systems exhibiting bursting phenomena, and may be closely related to that found in inclined layer convection.

It is hoped that our documentation of laminar bursting in a system distinctly different from inclined layer convection will stimulate new theoretical work on the problem. Experiments with higher η and with the outer cylinder rotating are also called for to determine whether subcritical instabilities emerge, in keeping with the predictions of Faisst and Eckhardt [4].

ACKNOWLEDGMENTS

We wish to thank Katie Hinko and Daniel Arking for their assistance in various phases of the data acquisition, and Robert Brodkey for the donation of some of the mechanical components of the apparatus. This work was partially supported by NSF REU Grant No. PHY-9912037 and PHY-0242665.

[1] C. D. Andereck, S. S. Liu, and H. L. Swinney, J. Fluid Mech. **164**, 155 (1986).
[2] H. A. Snyder, Int. J. Non-Linear Mech. **5**, 659 (1970).
[3] H. Faisst, Diplomarbeit thesis, Philipps-Universität Marburg, 1999.
[4] H. Faisst and B. Eckhardt, Phys. Rev. E **61**, 7227 (2000).
[5] A. Prigent, G. Gregoire, H. Chate, O. Dauchot, and W. van Saarloos, Phys. Rev. Lett. **89**, 014501 (2002).
[6] A. Prigent, G. Gregoire, H. Chate *et al.*, Physica D **174**, 100 (2003).
[7] P. W. Colovas and C. D. Andereck, Phys. Rev. E **55**, 2736 (1996).
[8] K. Coughlin and P. S. Marcus, Phys. Rev. Lett. **77**, 2214 (1996).
[9] C. F. Hamill, A. A. Predtechensky, E. Sha, and H. L. Swinney, 9th International Couette-Taylor Workshop, 1995.
[10] T. S. Sullivan and G. Ahlers, Phys. Rev. A **38**, 3143 (1988).
[11] J. Moehlis and E. Knobloch, Phys. Rev. Lett. **80**, 5329 (1998).
[12] P. Kolodner, S. Slimani, N. Aubry, and R. Lima, Physica D **85**, 165 (1995).
[13] K. E. Daniels, R. J. Wiener, and E. Bodenschatz, Phys. Rev. Lett. **91**, 114501 (2003).
[14] P. Matisse and M. Gorman, Phys. Fluids **27**, 759 (1984).
[15] O. Savas, J. Fluid Mech. **146**, 235 (1985).
[16] D. Coles, J. Fluid Mech. **21**, 385 (1965).
[17] M. M. Degen, I. Mutabazi, and C. D. Andereck, Phys. Rev. E **53**, 3495 (1996).
[18] H. Chaté and P. Manneville, Phys. Rev. Lett. **58**, 112 (1987).
[19] S. Ciliberto and P. Bigazzi, Phys. Rev. Lett. **60**, 286 (1988).
[20] S. Michalland, M. Rabaud, and Y. Couder, Europhys. Lett. **22**, 17 (1993).